

# Unifying positioning corrections and random number generations in silicon micro-strip trackers

Gregorio Landi<sup>a\*</sup>, Giovanni E. Landi<sup>b</sup>

<sup>a</sup> Dipartimento di Fisica e Astronomia, Universita' di Firenze  
Largo E. Fermi 2 (Arcetri) 50125, Firenze, Italy

<sup>b</sup> ArchonVR S.a.g.l.,  
Via Cisieri 3, 6900 Lugano, Switzerland.

July 6, 2023

## Abstract

The optimizations of the track fittings require complex simulations of silicon strip detectors to be compliant with the fundamental properties of the hit heteroscedasticity. Many different generations of random numbers must be available with distributions as similar as possible to the test-beam data. A fast way to solve this problem is an extension of an algorithm of frequent use for the center of gravity positioning corrections. Such extension gives a single method to generate the required types of random numbers. Actually, the starting algorithm is a random number generator, useful in a reverse mode: from non uniform sets of data to uniform ones. The inversion of this operation produces random numbers of given distributions. Many methods have been developed to generate random numbers, but none of those methods is directly connected with this positioning corrections. Hence, the adaptation of the correction algorithm to operate in both mode is illustrated. A sample distribution is generated and its consistency is verified with the Kolmogorov-Smirnov test. As final step, the elimination of the noise is explored, in fact, simulations require noiseless distributions to be modified by given noise models.

Keywords: Random number generations, Position Reconstructions, Center of Gravity,  $\eta$ -algorithm

PACS: 07.05.Kf, 06.30.Bp, 42.30.Sy

## 1 Introduction

The maximization of the resolution in track reconstruction [1] requires accurate eliminations of any systematic error present in the observations (hit reconstructions). Moreover, the inequalities of references [2, 3] impose careful accounts of the hit variances (heteroscedasticity) to reach the fit optimality. Evidently, the systematic errors disrupt those essential improvements. The easiest and frequently used positioning algorithm is the so called center of gravity (COG); the weighted average of some strip signals. Unfortunately, this algorithm, as any other, contains well known systematic errors [4], whose dangerous effects on momentum reconstruction are illustrated in reference [5]. However, such errors are disposable or reducible to negligible effects, these corrections are performed as described in [6]. The method generalizes the original algorithm (the  $\eta$ -algorithm) of reference [7] removing its intrinsic

---

\*Corresponding author. Gregorio.Landi@unifi.it

limitations. The definition [6] of the  $\eta$ -algorithm starts from a differential equation that transforms the non uniform COG distribution in an uniform one. As expected, the COG algorithm reconstructs the uniform distribution of hit-position on the strips in a non uniform distribution, clearly illustrated by the COG histogram. This distortion is due to the detector noise and the discretization of the signal distributions [4]. The reverse transformation to an uniform distribution compensate in large part the effects of the discretization, leaving outside only the noise effects that assumes the form of a narrow zero-average distribution [6]. Despite its flaws, the COG distortion in the histogram contain approximate signatures of the noise effects on the hit standard deviations. These signatures can be easily inserted in track-fitting gaining a substantial improvements of the track-parameters as demonstrated in [1, 8] (the lucky-model and the super lucky-model).

Actually, real reconstructions are not so simple as previously delineated. Instead, they require a set of different COG algorithms, each one containing a different number of strip signals in their calculations. Those COG algorithms have very different analytic and statistical properties [8] and must be tuned on the specific case. For simplicity, we often speak of this complex set of COG algorithms as a single element given that the mathematical procedure for their corrections are practically identical. However, we used the  $\eta$ -algorithm also well outside the correction of the COG systematic error. Its property allowed the extraction from the data of average signal distributions released by a minimum ionizing particle (MIP) on a set of nearby strips. Such distributions are essential to generate random distributions of correlated signals among the strips, the foundation of our simulations. In any case, the basic uses of the  $\eta$ -algorithm are the correction of the hit positions of incident MIPs on a layers of silicon strip detectors, layers whose sizes are many times the width of each strip. This setup suggests naturally the periodicity of the algorithm (with the period of a strip) and the use of the Fourier series to handle the mathematics of the problem. In its essence, the algorithm regenerates an uniform set of random numbers to an input of random numbers with the COG distribution [6]. The periodicity assures this correspondence for each strip of the layer. Apart a set of mathematical details we added to the  $\eta$ -algorithm generalization, the algorithm remains very similar to that used in many experiments. Those details allow to extend the structure of the algorithm well beyond its original aim. In particular, we are able to invert the algorithm and to obtain a random number generator with the COG distribution. Our interest was not addressed to generate random numbers, abundantly produced by the data tacking, but to its derivative that is connected to the average signal distribution released by the MIP [6, 9] in silicon detectors. As previously mentioned, just this derivative allowed the extraction from the data of another function very important for track fitting: the average fraction of the signal distribution collected by a cluster of strips, as a function of the hit position of the MIP. A theorem of reference [9] is pivotal to this extraction. This function implements also the two dimensional extension to our probability distributions (as reported in [8]), this extension is the base for the maximum likelihood search in track fitting [1, 5, 9]. To complete its use, the fraction of the signal distribution requires another essential element: the effective total signal released by the MIP and collected by the strips of our interest (three strips very often) to scale their fractions to the full value. Hence, to complete the simulations for track fitting it is required the production of many distributions of signal released by MIPs in double sided micro-strip detector [10, 11]. The theoretical forms of these distributions are supposed well known, they are usually defined as Landau distributions convoluted with Gaussian probability density functions (PDFs) of the noise, and they are often fitted in such a way. In reality the distributions are segments of convolutions, the true convolutions have infinite ranges.

Hence, given our need of only a part of the hit cluster, quite often the strip with the maximum signal and the two adjacent, these PDFs differ from the theoretical ones. In addition, for an easy consistency with the noise, we asked their expressions in ADC counts as our data. The cuts of the high energy side to reduce  $\delta$ -rays give a finite range to the PDFs, and the detection cuts eliminate the low energy sides of the distributions. The available forms of the PDFs are histograms with a finite set of data, and this has to be the model of our random number generator. Evidently, this type of problem has a well known solution: first produce the cumulative distribution function and invert it. The last step is not easy nor with a well

defined method. The appropriate method must be selected within the large number of different solutions present in literature, many of them can be found in ref. [12].

Similar necessity, requiring the generation of random numbers with a given empirical PDF, is very frequent. Data analysis are important sources of empirical PDF that have to be used in the construction of realistic simulations. Histograms with a finite number of events (often not too many) are their usual forms. Even if their fundamental probability models are known, experimental details modify the models in substantial way and render the analytical models of doubtful use in the production of realistic data sets or too complex.

For the special physical properties of our reconstructions, the developments of the  $\eta$ -algorithm looks particularly efficient for this class of problems. Although we illustrated the method in references [4, 6, 9, 13], those illustrations are not effective to describe the present use. There, the main task is the hit position reconstructions, and this obscures the extraction of the relevant steps. Here, we concentrate on the procedure essential for this application. Section 2 describes the details of this unification, in Section 3 the data generation is illustrated with the intrinsic difficulties of our selected test distribution. The Kolmogorov-Smirnov test of the generated distribution is in Section 4. Two methods for noise filtering are discussed in Section 5. Section 6 contains the summary and the conclusions.

## 2 Definition of the problem

A given PDF defines the distribution of the generated random numbers, the PDF must have finite range, can be expressed in any scale and has to be always different from zero. Our model distribution is a set of signals release by a MIP in two sided micro-strip detectors. The data were acquired with a test-beam [11] in CERN by a tracker with five detection layers. Our data cover many incident directions and two different types of detectors. For this illustration, we use the side with higher noise and orthogonal incidence. All the hits of the detector layers are collected together to increase the statistics, and the charges detected by three strips are reported on an histogram (normalized and divided by the bin size) often indicated as frequency polygon. The frequency polygon will be called empirical PDF or simply PDF, and reported in fig. 1.

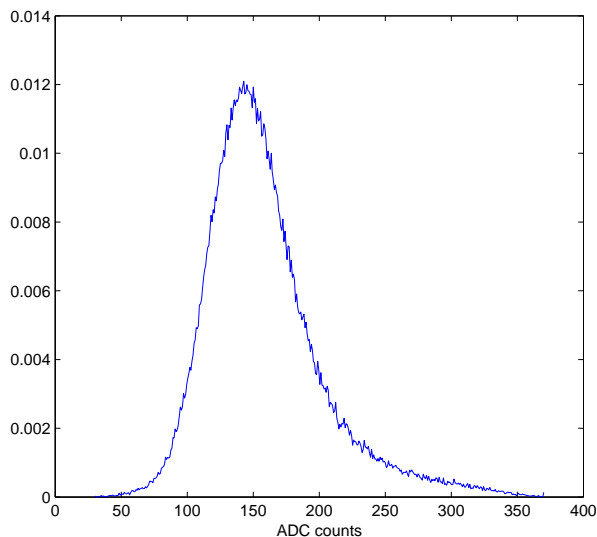


Figure 1: Empirical PDF for the signal released in three strips by an incident MIP (ADC counts, 215613 events, bin size 0.8 ADC counts)

The data are distributed from 30 ADC counts to 370 ADC counts and the PDF is different from zero in all the interval as required. This type of interval is unpractical and it is better to transform the interval in a standard one defined from  $-1/2$  and  $+1/2$  with the trivial transformations  $x = (x' - 200)/340$  (and  $y = y' * 340$ ), this interval coincides with that used for our COG corrections where we normalize all the lengths with the strip width. With this quite simple scaling of the PDF, the algorithm can be used in any case. Due to these definitions, the dimensions in the plots become pure numbers and do not require special indications.

Reference [4] generalizes the  $\eta$ -algorithm of reference [7] extending it to a set of different COG algorithms with any number of strips in the COG definition, well beyond the two strips accounted in [7], and releasing its very complicated sorting of the strips. The necessity of using COG algorithms with a different number of strips is due to the substantial differences in systematic errors and probability distributions (as in [8] and therein references) of those algorithms, they must be fine tuned on the applications. The generalized  $\eta$ -algorithm eliminates the systematic errors of the COG algorithms, but, for the use at its best as in [8] (also with the insertion of an approximate account of the hit heteroscedasticity to improve the fits), the algorithm must be completed with some details illustrated in references [4, 6]. Due to these generalizations, we have to handle events with their COG positions outside the reference interval  $-1/2, +1/2$ ; the three strip COG and the four strip COG have often such events. The selected solution was the extension of the supposed uniform illumination on a single virtual strip to a supposed uniform illumination on an infinite array of strips. Thus, the data escaping from a strip are recovered in the adjacent strips defining a reproducible rule to handle uniformly in all these cases. This simple modification introduces important consequences on the method to handle the COG probabilities: the periodicity. In fact, to handle the hits on a large array of micro-strips, the algorithm must be extended to work identically on any strip cluster of an array with any number of micro-strips. The periodicity eliminates one of the Kolmogorov axioms of probability [14]: the normalization of the distribution. We have to limit to a weaker condition of normalization on a strip. We encountered the necessity of this weaker condition also in reference [8] again for the extension of probabilities to detectors of any size.

However, the fundamental gain of the periodicity is the use of the Fourier Series to solve the equations and the possibility to invert the COG equations for any impact point. These properties can be extended to the present problem as shown in figure 2. Here, we have no underlying position calculation and we are free from the complications due to the selection of the integration constant of the differential equation. The selection of this constant in positioning problem is easy only in the case of symmetrical set up, and this is an essential limit of reference [7].

The change of variables in a PDF is given by the equation:

$$\Gamma(\varepsilon) \frac{d\varepsilon}{dx} = \Gamma^p(x), \quad (1)$$

the probability  $\Gamma(\varepsilon)$  is transformed in a distribution of  $x$  with a probability  $\Gamma^p(x)$ . The uniform distribution is given by  $\Gamma(\varepsilon) = 1$ , and the function  $\varepsilon(x)$  has a uniform distribution. The equation 1 becomes the first order differential equation:

$$\frac{d\varepsilon}{dx} = \Gamma^p(x) \quad (2)$$

with solution:

$$\varepsilon(x) = -\frac{1}{2} + \int_{-1/2}^x \Gamma^p(y) dy. \quad (3)$$

The integration starts at  $-1/2$  to keep track of the single period of our interest, and evidently contains the generalized cumulative distribution of  $\Gamma^p(x)$ . The assumption of normalization on a strip allows to rewrite equation 3 in the form:

$$\varepsilon(x) = x + \int_{-1/2}^x [\Gamma^p(y) - 1] dy \quad (4)$$

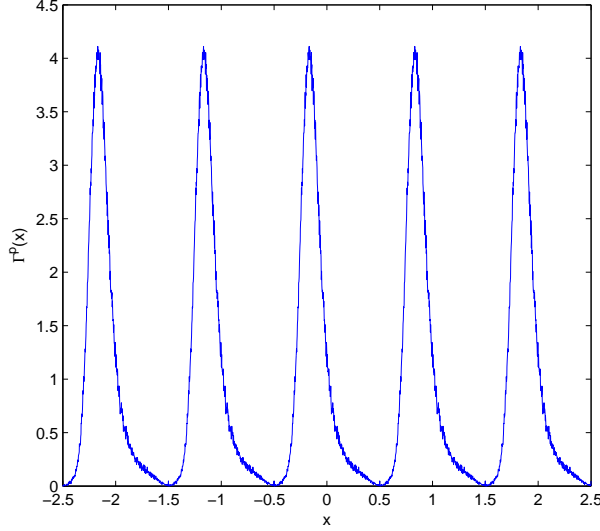


Figure 2: Periodic empirical PDF in the transformed coordinate system ( $\Gamma^p(x)$ )

It is easy to show that the integral in equation 4 is periodic with period 1. In fact, the contribution of all the complete periods, contained in the interval  $-1/2 \vdash x$ , are zero due to the normalization of  $\Gamma^p(x)$  on a period. The integration on the remaining part of the interval is identical in any period. The Fourier Series becomes:

$$\begin{aligned} \varepsilon(x) &= x + \sum_{k=-\infty}^{+\infty} \alpha_k e^{2\pi i k x} & \alpha_k &= \int_{-1/2}^{1/2} [\varepsilon(y) - y] e^{-2\pi i k y} dy \\ \alpha_k &= \frac{1}{2\pi i k} \int_{-1/2}^{1/2} [\Gamma^p(y)] e^{-2\pi i k y} dy \quad k \neq 0 & \alpha_0 &= - \int_{-1/2}^{1/2} \Gamma^p(y) y dy \end{aligned} \quad (5)$$

The variable  $\varepsilon$  coincides with  $x$  at  $-1/2$  and  $+1/2$  and at the end of any other period. The second line of the equation 5 is obtained with an integration by part of  $\varepsilon(x) - x$  of equation 4. The limitation on  $k$  in numerical calculation operates as a filter that suppresses part of the noise always present in empirical PDF.

The complex discussions of references. [6, 13] were specific for the position reconstructions where systematic errors must be reduced at their minima. In that case the integration constant of the differential equation must be an exact position (or the best approximation) and it has to be extracted from the set of data with unknown relations with the true impact points (excluding the trivial case of symmetric signal distributions).

### 3 The generator of random numbers

Equation 5 clearly illustrates the gain of the imposed periodicity, the function  $\varepsilon(x)$  has a linear increasing component and a periodic part. The sum of these two components has everywhere a positive derivative (figure 2). Thus,  $\varepsilon(x)$  can be inverted in another linear increasing part and a periodic part:

$$x(\varepsilon) = \varepsilon + \sum_{m=-\infty}^{+\infty} \beta_m e^{2\pi i m \varepsilon} \quad \beta_m = \int_{-1/2}^{+1/2} [x(\varepsilon) - \varepsilon] e^{-2\pi i m \varepsilon} d\varepsilon \quad (6)$$

In its form equation 6 is useless because we do not know  $x(\varepsilon)$ , but we know  $\varepsilon(x)$  and transforming the integration variable to  $x$ , the expression for  $\beta_m$  becomes:

$$\begin{aligned}\beta_m &= \int_{-1/2}^{+1/2} [x - \varepsilon(x)] e^{-2\pi i m \varepsilon(x)} \frac{d\varepsilon}{dx} dx \\ &= \int_{-1/2}^{+1/2} [x - \varepsilon(x)] e^{-2\pi i m \varepsilon(x)} \Gamma^p(x) dx\end{aligned}\quad (7)$$

where in the last line of equation 7 we introduced equation 1. The insertion of equation 4 gives:

$$\beta_m = - \int_{-1/2}^{+1/2} dx \int_{-1/2}^x dy [\Gamma^p(y) - 1] e^{-2\pi i m \varepsilon(x)} \Gamma^p(x) \quad (8)$$

Other forms for  $\beta_m$  can be obtained integrating by parts equation 8 (the exponential and  $\Gamma^p(x)$  are proportional to the  $x$ -derivative) and remembering the boundary conditions  $\varepsilon(\pm 1/2) = x(\pm 1/2) = \pm 1/2$ :

$$\beta_m = \frac{1}{2\pi i m} \int_{-1/2}^{+1/2} \exp[-2\pi i m \varepsilon(x)] dx \quad m \neq 0 \quad \beta_0 = \int_{-1/2}^{+1/2} x \Gamma^p(x) dx \quad (9)$$

Evidently, the amplitude  $\beta_0$  coincides with the first momentum of the PDF as is clear in equation 6. In fact, for  $m = 0$  the integral of  $\varepsilon$  is zero being an odd function, thus the sole integration of  $x d\varepsilon/dx$  remains and the use of equation 2 gives the result of equation 9.

These different expressions are useful in real calculations. The unlimited sums in the Fourier series with the different forms of  $\beta_n$  give identical results, but the finite approximations can show different sensitivity to the details of the PDF. We will call  $\pm L_\alpha$  and  $\pm L_\beta$  the extremes of the sums of equation 5 and equation 6. These finite values tend to introduce very small shift of the boundary conditions used in equation 9, but due to periodicity these are irrelevant or easily recovered.

### 3.1 Numerical calculations

The integration of equation 3 is numerical, and performed on a histogram with very small bin-size (much smaller than that of figure 2). Due to the non decreasing property of the integral, the small bin-size is able to follow accurately the form of  $\Gamma^p(x)$ . Identical histogram is used also in equation 5 to calculate  $\alpha_n$  with the limits  $\pm L_\alpha$ . From now on  $\varepsilon(x)$  will be given by its Fourier series. Identical steps, but with COG histograms, allow to obtain expressions to be used in [1, 8] for the lucky-model and the super lucky-model; in fact, the derivatives of similar Fourier series give analytical forms of  $\Gamma^p(x)$  reproducing the COG histograms for the use in improving the track fitting.

The value of  $L_\alpha$  operates as an ideal low-pass filter that suppresses the fluctuations always present in empirical PDF and those due to small bin size of the numerical integration. Symmetrically, a too low value of  $L_\alpha$  can eliminate important details of the PDF, hence, some care can be exerted on this selection.

The inverse function  $x(\varepsilon)$  is obtained with the  $\beta_m$  given by equation 8, and the limits  $\pm L_\beta$ . The use of a low value of  $L_\beta$  generates random numbers with a set of  $L_\beta$  narrow peaks. The peaks decrease in amplitude at increasing  $L_\beta$  and are smeared by the randomness of the  $\varepsilon$  values, but they remain visible. These fluctuations are typical of Fourier Series when the convergence of the series is slow [15]. The slow convergence is due to large values of the transformed function, essentially the inverse of the distribution of figure 2. The values around  $\pm 1/2$  are very small and their inverses become very large. To suppress almost completely these fluctuations, the large  $L_\beta$  must be reinforced summing the Fourier Series with the method of arithmetic mean ( Cesaro summation ) that is able to suppress the Gibbs effect around discontinuities [15]. The remaining oscillation (if any) are invisible also enlarging at the maximum the following figures. In its finite form the Cesaro summation is equivalent to the triangular filter  $(1 - |m|/L_\beta)$  (Bartlet window in digital filters) applied to the  $\beta_m$ -amplitudes and centered at  $m = 0$ .

The arithmetic mean redefines the form of the sequence of functions converging to the Dirac  $\delta$ -function for  $N \rightarrow \infty$ . The standard sum produces functions of the form  $F_N(u) = \sin[(N + 1/2)u/2]/\sin(u/2)$ . At any  $N$ , these functions have large positive and negative oscillations around the peak in  $u = 0$  with  $1/u$  as weak smearing. The Cesaro summation produces the set of converging functions to the Dirac  $\delta$ -function of the form  $C_N(u) = [\sin(Nu/2)]/[2N \sin(u/2)^2]$ . Now the oscillations are strongly damped by  $1/u^2$  and are always positive. A drawback is the slower increase of the peak, in fact,  $F_N(0) = N + 1/2$  and  $C_N(0) = N/2$ . These different types of convergence are relevant for finite sums.

The complexity of the  $\beta_m$  calculation is not visible in equation 9, but can be clearly evidenced by the following expression:

$$\beta_m = \frac{1}{2\pi i m} \int_{-1/2}^{+1/2} \exp[-2\pi i m \varepsilon(x)] \frac{dx}{d\varepsilon} d\varepsilon \quad \frac{dx}{d\varepsilon} = \frac{1}{\Gamma^p(x(\varepsilon))} \quad (10)$$

The function  $1/\Gamma^p(x(\varepsilon))$  is reported in figure 3, the other two curves (all almost coinciding but with different heights at  $\pm 1/2$ ) are the numerical derivatives of  $x(\varepsilon)$  obtained from equation 9 with  $L_\beta = 200$  and  $L_\beta = 40$ . All these curves are functions of  $\varepsilon$ . The origin of the two peaks is due to the small values of  $\Gamma^p(x)$  at  $x \approx \pm 1/2$ . To produce an uniform distribution, the cumulative distribution  $\varepsilon(x)$  is forced to compress the  $x$ -regions of low probability in a narrow  $\varepsilon$ -region enhancing the steepness of the peaks. For their good reproduction,  $L_\beta$  must be around 200 or higher. The low values of  $\Gamma^p$  towards  $\pm 1/2$  render this case more complex than our previous use of this inversion for the COG problems. In micro-strip detectors, the COG probabilities have restricted regions of low probabilities generating negligible disturbances.

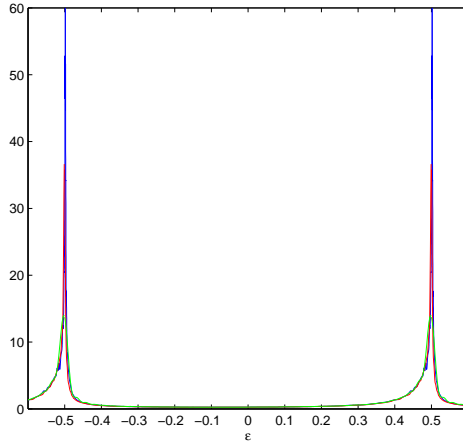


Figure 3: The blue line is  $1/\Gamma^p(x(\varepsilon))$  the inverse of original PDF with its large values at  $\pm 1/2$ , the other two curves are  $dx(\varepsilon)/d\varepsilon$  obtained with  $L_\beta = 200$  (the red line) and with  $L_\beta = 40$  (the green line).

An interesting comparison is with the  $\Gamma^p(x)$  obtained by the  $d\varepsilon(x)/dx$  as in equation 2 and the  $(dx(\varepsilon)/d\varepsilon)^{-1}$  plotted as function of  $x(\varepsilon)$ , here  $x(\varepsilon)$  is calculated with  $L_\beta = 200$ . The second function is the form of the data PDF given by this random data generator. Figure 4 illustrates the excellent agreement of the two curves. This is not surprising given that  $x(\varepsilon)$  is the inverse function of  $\varepsilon(x)$  thus  $\varepsilon(x(\varepsilon)) = \varepsilon$ . The root mean square of the difference  $\varepsilon(x(\varepsilon)) - \varepsilon$  on a period is  $1.7 \cdot 10^{-3}$ .

As final test, figure 5 reports the histograms (frequency polygons) of figure 1 and the similar histogram with the data produced by this generator and reported to the original scale. The overlap is complete.

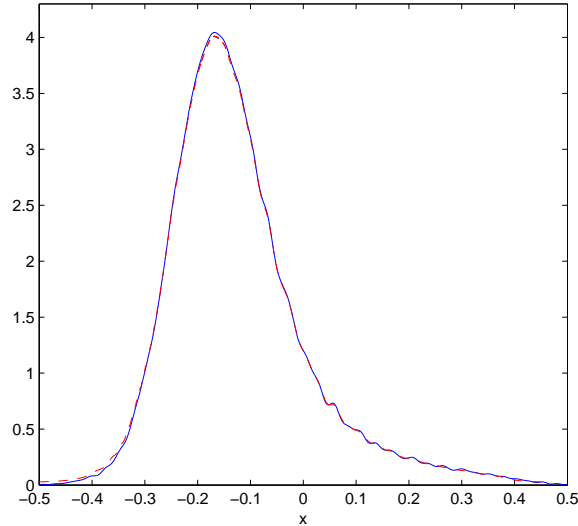


Figure 4: The blue line is  $\Gamma^p(x)$  as given by the left side of equation 2 (essentially the data plot with a filter on the main fluctuations), the red dashed line is the expression  $(dx(\varepsilon)/d\varepsilon)^{-1}$  plotted as a function of  $x(\varepsilon)$  with  $L_\beta = 200$ .

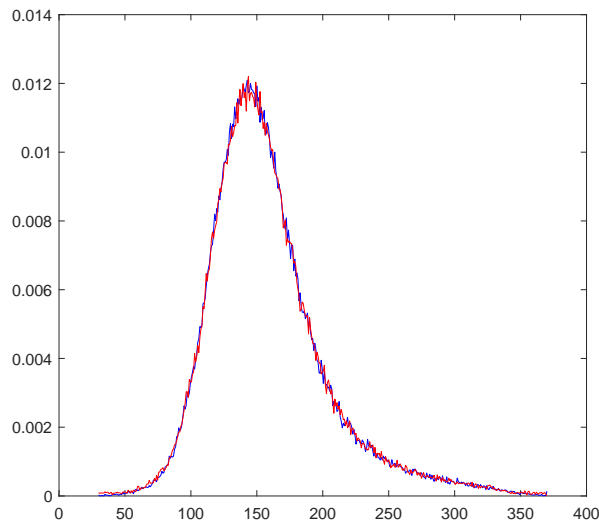


Figure 5: Histogram of the original data (the blue line) and the histogram of the generated data (the red line) reported to the right scale. The two histograms have identical number of data, normalized and divided by the bin size (0.8 ADC counts).

### 3.2 PDF with long low probability tails

We showed the difficulty introduced by these relatively low tails of the PDF. Longer tails with lower probability will be dangerous for this method. We can get around this problem sectioning the tails and treating them as independent PDF to be handled as described above. In this case, the data generation proceeds in two steps. At the first, the interval 0-1 is divided in two parts (or more if required) a main interval equal to the cumulative PDF of the main part, and a remaining interval equal to the cumulative PDF of the tails. The extraction of a uniform random number in the interval 0-1 selects which PDF generators must be used (Russian roulette).



## 4 Kolmogorov test

Let us test the quality of our cumulative distribution function  $\varepsilon(x)$  respect to the empirical cumulative distribution function obtained by the data. We have to rearrange the data to obtain an ordered statistics  $\{o_1, o_2 \dots o_N\}$  sorting the data with increasing values. This reorder renders the empirical cumulative distribution quite simple:  $F(o_k) = k/N$ . A Kolmogorov theorem [16, 17] states that for  $N \rightarrow \infty$  the probability of  $\sqrt{N} \sup_i |F(o_i) - \varepsilon_1(o_i)| \leq t$  converges to  $k(t)$ . Where  $\varepsilon_1(x) = \varepsilon(x) + 1/2$  to recover the initialization of  $\varepsilon(-1/2) = -1/2$ , and to report  $\varepsilon_1(x)$  spanning the interval  $0 \vdash 1$ . More precisely, the probability  $\mathbf{P}(x)$  is:

$$\lim_{N \rightarrow \infty} \mathbf{P}(\sqrt{N} \sup_i |F(o_i) - \varepsilon_1(o_i)| \leq t) = k(t) = 1 - 2 \sum_{j=1}^{+\infty} (-1)^{j-1} \exp(-2j^2 t^2) \quad (11)$$

For our  $N$ -values well above 200000 we can use the asymptotic results and the maximum of our differences, scaled by  $\sqrt{N}$ , is 0.383. For  $t = 0.383$  it is  $k(0.383) \approx 0.0015$ , or a probability around 0.15% to find a better cumulative function.

With small modification of Smirnov [17] (a factor  $1/\sqrt{2}$ ), equation 11 can be applied also to our generated set of random data of figure 5, but with a negative result. The test is too sensible to the almost invisible differences of the low probability parts of the distributions. We illustrated this problem in figure 3 where the two high peaks are not well reproduced. The differences are limited to a small number of events, invisible in the plots, but able to move the test toward the rejection region. To generate distributions fully accepted by the Kolmogorov-Smirnov test, we have to proceed as in subsection 3.2, i.e. divide the probability distribution in three parts. A central part with almost all the events, and two lateral side with relatively few events. Applying the described algorithm at the central part and the two lateral parts, assembled together to produce a single PDF, it is easy to produce accepted distributions. The differences among the plots reported in figure 5 and in the following figure 8 are invisible to the eye,

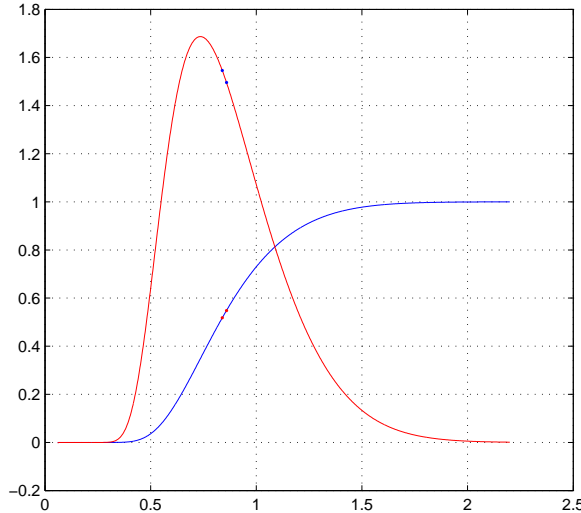


Figure 6: Plots of the Kolmogorov cumulative distribution probability of the asymptotic difference of maximum  $\mathbf{P}(x)$  (blue line) and the PDF of  $\mathbf{P}(x)$  (red line). The two dots are the values of  $\mathbf{P}(x)$  for two different generations of random data. One of the two is reported in figure 8.

The separation of the low probability data and the high probability data, produces sets of random numbers easily accepted by the Kolmogorov-Smirnov test. Equation 11, for a value of the argument

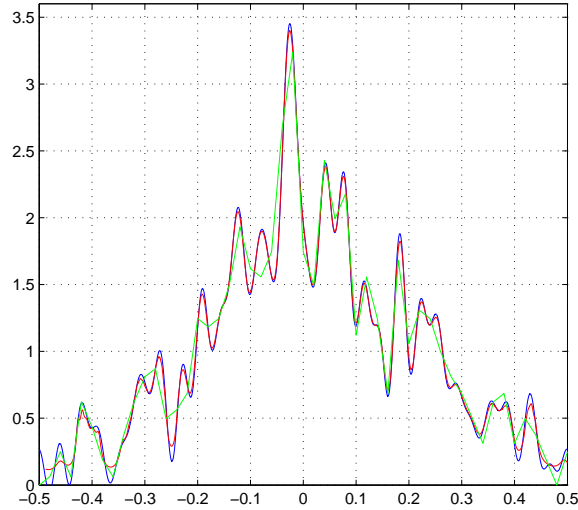


Figure 7: Plots of the low probability distributions, blue line  $(d\varepsilon/dx)$ , red line the reconstructed distribution  $(dx(\varepsilon)/d\varepsilon)^{-1}$  the green line is the histogram of the data

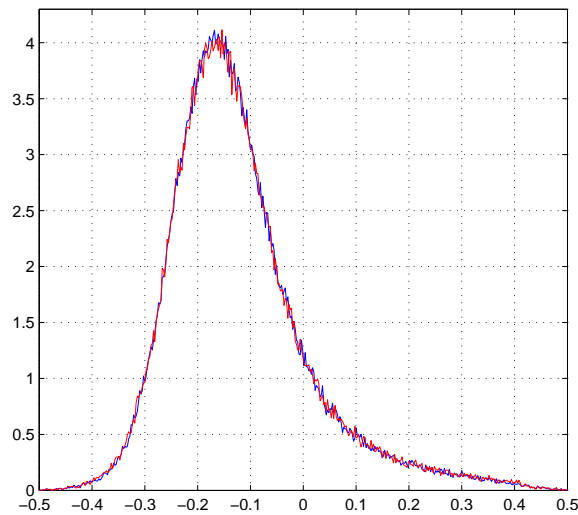


Figure 8: Plots of the full probability distributions (low+high) , blue line is the histogram of the data. The red line is the histogram of the generated random numbers accepted by the Kolmogorov test

0.859 of our example generation, gives a probability of 0.548 well below the 0.95, boundary of the confidence level, and 0.859 is among the most probable values of these differences as shown in figure 6. Figure 7 is the plot of the low probability parts and figure 8 illustrates the comparison of the histogram of the data with the generated random numbers accepted by the test.

## 5 Noise suppression

### 5.1 Lucy-Richardson method

The analytical form given by the equation 5 rises the possibility to extract the noiseless form from the noisy distribution of figure 1. The large set of data reduces strongly the noise fluctuation of the histogram

of figure 1, although noise components survive. A variation of the method of Lucy and Richardson [18, 19] will be use to reduce those components.

In principle, the noise effect is a convolution of the noiseless signal with the Gaussian noise distribution. We tested the noise distribution in our data exploring the random signals of the strips outside the signal clusters. The probability of another hit in these strips is evidently negligible and the random signals are essentially noise. These random signals are well reproduced by a Gaussian PDF. The Fourier transform of a convolution gives an apparent strategy to clean the noise, but further details must be consider. The first one is the finite range of our data set. For an analytical function, even of finite range, the convolution with a Gaussian gives a function different from zero on all the real line, with negligible values on the tails. These tails are essential to give the correct convergence at high frequency so sustaining the division by another Gaussian (the Fourier transform of a Gaussian noise). Instead, a finite range distribution has a Fourier transform that goes to  $\infty$  as  $1/\omega$ . Multiplication by  $\exp(\omega^2)$  generates an explosion of the high frequency and a very oscillating result. With some care, the Lucy-Richardson method allows an analytical solution for our case.

$$\Gamma^p(x) = \Pi(x) \int_{-1/2}^{+1/2} P(x-y)\Psi(y)dy \quad (12)$$

This equation is essentially that of reference [18],  $\Gamma^p(x)$  is the signal corrupted by the noise, and  $P(x-y)$  is the Gaussian noise PDF with variance  $\sigma^2$ ,  $\Psi(y)$  is the noiseless distribution and  $\Pi(x)$  is the interval function ( $\Pi(x) = 1$  for  $|x| \leq 1/2$ ,  $\Pi(x) = 0$  for  $|x| < 1/2$ ). In addition to the Gaussian noise,  $\Gamma^p(x)$  contains the noise due to the finiteness of the data sample. This last noise is difficult to be modeled and must be dealt empirically in a more or less reasonable methods.

Consistently with our assumption on  $\Gamma^p(x)$ , we will assume an identical periodicity also for  $\Psi(y)$ . Inserting the Fourier Series for  $\Gamma^p(x)$  (amplitudes  $\gamma_n = 2\pi i n \alpha_n$  and  $\gamma_0 = 1$ ) and  $\Psi(y)$  (with amplitudes  $\gamma_n^0$ ), equation 12 becomes:

$$\gamma_n = \sum_k N_{n,k} \gamma_k^0 \quad N_{n,k} = \int_{-1/2}^{+1/2} \exp[-2\pi i (nx - ky)] P(x-y) dx dy \quad (13)$$

The integrals of equation 13 are not too complex, and MATHEMATICA [20] is able to do them. The off-diagonal terms are irrelevant and the diagonal terms alone are worth of attention, they have the expression:

$$N_{k,k} = \sqrt{\frac{2}{\pi}} \sigma \left[ e^{-1/2\sigma^2} \cos(2k\pi) - 1 \right] + \frac{1}{2} e^{-2(k\pi\sigma)^2} \left\{ 4k\pi\sigma^2 \operatorname{erfi}(\sqrt{2}k\pi\sigma) + 2\operatorname{real} \left[ (1 - 2ik\pi\sigma^2) \operatorname{erf} \left( \frac{1 - 2ik\pi\sigma^2}{\sqrt{2}\sigma} \right) \right] \right\} \quad (14)$$

As  $k$  increases  $N_{k,k}$  has an almost  $1/k$  decrease (as expected), very different from the rapid decrease of a Gaussian term as shown in figure 9. For  $k \leq 11$ ,  $N_{k,k}$  coincides with the pure Gaussian correction. In spite of this, the direct use of  $N_{k,k}$  in equation 12 is very unrealistic. The noise introduced by the histogram fluctuations are similar to a white noise with frequency spectrum that further attenuates the decrease of  $\gamma_k$  with  $k$ . The large number of events assures a reliability of the first  $\gamma_k$  amplitudes, on which we can apply equation 12. Neglecting the frequencies with  $k$  greater than 9 or 10, the strip noise suppression gives the result of figure 10.

The plausibility of the solution can be tested approximating the distributions as a Gaussian PDFs (at least around the maxima), in this case the noise suppression is an easy procedure  $\sigma_t^2 = (\sigma_0^2 + \sigma_n^2)$  and the full width at half maximum of the noisy PDF is  $\sigma_t \sqrt{8 \ln(2)} = 0.211$  giving a  $\sigma_t = 0.0896$ . Due to the data strip-noise  $\sigma_n = 8\sqrt{3}/340$ , than the noiseless  $\sigma_0$  would be 0.0798 and a noiseless full width at half maximum of 0.188. The full width at half maximum of the red line in figure 10 is 0.180 that is very similar to the one for a Gaussian function.

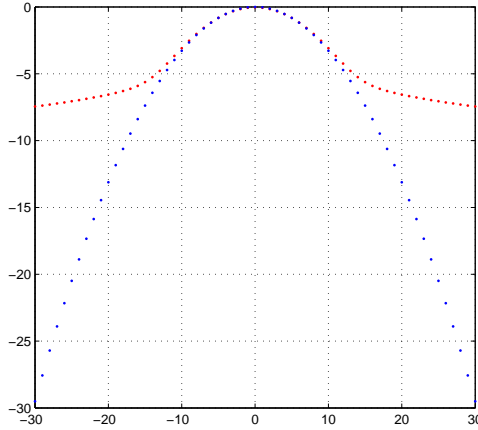


Figure 9: The red dots are the  $\log(N_{k,k})$  for the noise of  $8\sqrt{3}$  ADC counts of the sum of three strip signals. The blue dots are the the logarithms of the corresponding pure Gaussian factors.

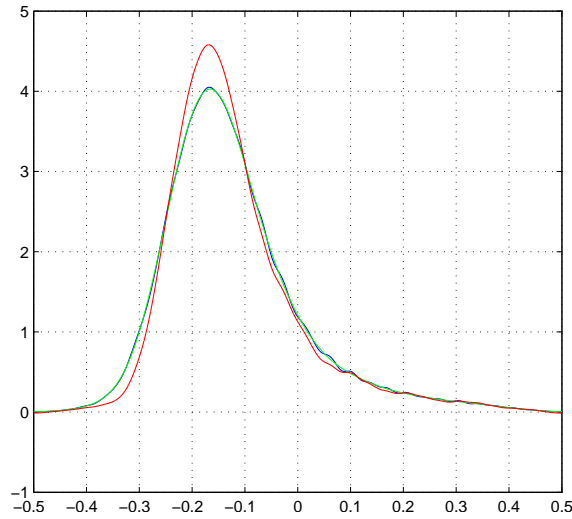


Figure 10: The red line is a possible noiseless result, the blue line is the original PDF, and the green line is given by the full reapplication of the noise to  $\gamma_n^0$  at all the amplitudes.

## 5.2 Wiener filter

Another interesting method to compensate the noise is the use of the Wiener filter [21]. The Wiener filter executes a deconvolution of the signal keeping into account also the additional noise due to the signal elaboration (as the histogram construction). The insertion of this additional noise moderates the effects of the division by the rapidly decreasing amplitude of the Gaussian Fourier transforms. As shown previously, also the expressions of the equation 14, with their linear decrease, create rapidly strong oscillations with a small number of  $k$ -terms. To have a reasonable result we have to add a drastic limit to the  $k$ -maximum. The Wiener filter operates with the following equation for the Fourier series amplitudes:

$$\gamma_k^0 = \gamma_k \frac{(N_k^g)^*}{|N_k^g|^2 + S_k}. \quad (15)$$

The terms  $N_k^g$  are the Gaussian amplitudes of figure 9, the parameters  $S_k$  are the ratios of the mean power of the additional noise (the detection/elaboration noise) to the mean power of the signal. We do not

invest effort to calculate the  $S_k$  amplitudes and, as usual, we assume a constant value for any  $k$ -term, as having to do with a white noise. The  $S_k = 0.01$  gives a result very similar to the previous development as illustrated in figure 11. The effect of the terms  $S_k$  in equation 15 are very clear: they suppress the effects

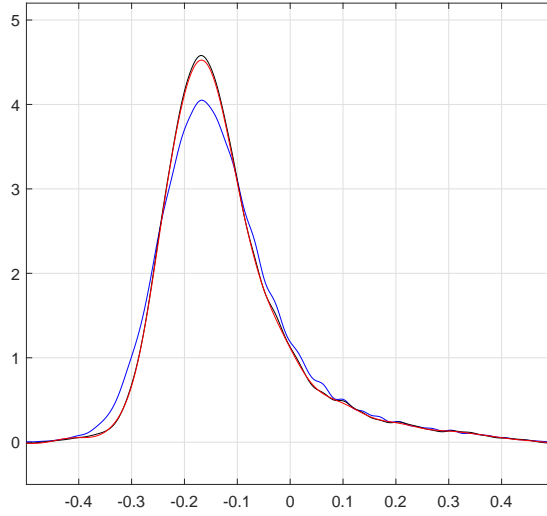


Figure 11: The red line is the result of the Wiener deconvolution, the blue line is the original PDF, and the black line is the previous filtering.

of the small amplitudes  $N_k^g$ . Equation 15 has the general form with the complex numbers  $N_k^g$ . In our case, the  $N_k^g$  are real numbers for the symmetry of the Gaussian PDF. The constant  $S_k$  is not critical and the filtered distribution has very few shifts for values around 0.01. Instead the value 0.001 starts to show substantial oscillations in the filtered distribution.

The generations of the "noiseless" random signals now begin from the distributions of figure 11 going back to equation 7. The filtered  $\alpha_n^0$  is given by  $\alpha_n^0 = \gamma_n^0 / (2\pi i n)$  composing the series of  $\epsilon^0(x)$ .

### 5.3 Empirical noise "suppression"

An empirical method can be used to reduce the noise effects, we used this in reference [9]. The histogram of figure 1 is shrunk by the three strip noise supposing the core of the histogram to be a Gaussian PDF. The amplitudes were those reported at the end of subsection 5.1. The shrinking operates also on the total interval of the data, reducing it to 303 ADC counts. The new histogram is used to construct the random number generator from equation 4. The random numbers, simulating the strip noise, are generated starting from equation 4 and a histogram of strip signals for strips far from those interested by the MIP signals (exclusively noise with high probability). This selection accounts also any deviation from a pure Gaussian noise, for example the truncation noise due to the ADC conversion, and has finite range. The simulated MIPs data produce histograms of single strip signals with excellent overlaps on those of the real MIP data.

## 6 Conclusions

The account of the hit heteroscedasticity introduces a complex interplay among the center of gravity as positioning algorithm, its histograms, the signals collected by the strips and the hit variances to be inserted in the track fitting. To test and isolate those relations, many sets of simulations are required. The standardization of the methods for random number generations strongly alleviated this heavy work and

could allow to isolate other useful relations. The unification in a single algorithm the correction of the systematic error of center of gravity algorithm and the generation of other necessary random numbers is an excellent step in that direction. The algorithm for the correction of the center of gravity positioning was carefully discussed in previous publications, but some specific aspects of this correction obscures its usefulness for the present task. The periodicity, imposed by layers of micro-strips, suggests the use of the Fourier series and its powerful shortcuts. The oscillations produced by the small values of the sample of probability distributions can be cured in various ways, increasing the numbers of Fourier amplitudes, using the Cesaro summation or splitting the probability distribution in sections. This last strategy is able to generate sets of random numbers accepted by the Kolmogorov-Smirnov test, although these distributions show no appreciable differences with generations obtained without that splitting. Evidently, the low probability section is strongly modified by the small number of events and their large fluctuations. The test is very sensitive to those fluctuations, but in practical use the sectioning can reasonably be neglected. As final development, the filtering of the noise in the original distribution is explored with two different methods, the Lucy-Richardson method and the Wiener method with similar results. The plausibility of the noise filtering is verified approximating the cores of the distributions as Gaussian distributions. In this case the noise suppression is an easy analytical task, and it shows a clear consistency with the more elaborated methods.

### Abbreviations

The following abbreviations are used in this article:

ADC Analog-to-Digital Converter  
 COG Center of Gravity  
 MIP Minimum Ionizing Particle  
 PDF Probability Density Function

### References

- [1] Landi G.; Landi G. E. Beyond the  $\sqrt{N}$ -limit of the least squares resolution and the lucky-model Instruments 2022, 6, 10. <https://doi.org/10.3390/instruments6010010>
- [2] Landi G.; Landi G. E. The Cramer-Rao inequality to improve the resolution of the standard least-squares method in track fitting. Instruments **2020**, 4, 2. <https://doi.org/10.3390/instruments4010002>
- [3] Landi G.; Landi G. E. Generalized Inequalities to Optimize the Fitting Method for Track Reconstruction. Physics 2020, 2, 608-623. <https://doi.org/10.3390/physics2040035>
- [4] Landi, G. The center of gravity as an algorithm for position measurements Nucl. Instr. and Meth. A **485** (2002) 698 arXiv:1908.04447 [physics.ins-det] <https://arxiv.org/abs/1910.04447>.
- [5] Landi, G.; Landi G. E. Optimizing momentum resolution with a new fitting method for silicon-strip detectors INSTRUMENTS **2018**, 2, 22
- [6] Landi, G. Problems of position reconstruction in silicon microstrip detectors Nucl. Instr. and Meth. A **554** (2005) 226.
- [7] Belau, E.; Klanner, R.; Lutz, G.; Neugebauer, E.; Seebrunner, H.J.; Wylie, A. Charge collection in silicon strip detector. Nucl. Instrum. Methods Phys. Res. A 1983, 214, 253-260.
- [8] Landi, G.; Landi, G.E. Probability Distributions for Track Fitting and the Advanced Lucky Model. Physics 2022, 4, 1026-1049. <https://doi.org/10.3390/physics4030068>

- [9] Landi G.; Landi G. E. Improvement of track reconstruction with well tuned probability distributions *JINST* 9 2014 P10006. arXiv:1404.1968[physics.ins-det] <https://arxiv.org/abs/1404.1968>
- [10] Landi G., Landi G. E. Silicon Microstrip Detectors Encyclopedia 2021, 1, 1076-1083. <https://doi.org/10.3390/encyclopedia1040082>.
- [11] Adriani, O.; Bongi, M.; Bonechi, L.; Bottai, S.; Castellini, G.; Fedele, D.; Grandi, M.; Landi, G.; Papini, P.; Ricciarini, S.; et al. In-flight performance of the PAMELA magnetic spectrometer. In Proceedings of the 16th International Workshop on Vertex Detectors, (PoS(Vertex 2007)048), Lake Placid, NY, USA, 23-28 September 2007.
- [12] Devroye, L. "Non Uniform Random Variate Generation", Springer-Verlag, New York 1986.
- [13] Landi, G.; Landi, G.E. "Asymmetries in Silicon Microstrip Detectors and the Lorentz Angle" [phys.ins-det] arXiv:1403.4273
- [14] Gnedenko, B. V. "The Theory of Probability and Elements of Statistics" (AMS Chelsea Publishing -Providence Rhode Island )
- [15] Tolstov, G.P. "Fourier Series" (Prentice-Hall, inc. Englewood Cliff, New Jersey 1962)
- [16] Kolmogorov, A. "Sulla determinazione empirica di una legge di distribuzione" *Giornale dell'Istituto Italiano degli Attuari*. 4 83-91 1933
- [17] Ivchenko, G.; Medvedev, Yu. *MATHEMATICAL STATISTICS*-Moscow-URSS-1990
- [18] Lucy, L.B. "An iterative technique for the rectification of observed distributions" *Astronom. J.* 79 (1974) 745
- [19] Richardson, W.H. "Bayesian-Based Iterative Method of Image Restoration" *J.Opt.Soc.Am.* 62 (1972) 55
- [20] MATHEMATICA 6 Wolfram Inc. Champaign IL, USA
- [21] Wiener, N. "Extrapolation, Interpolation, and Smoothing of a Stationary Time Series", The M. I. T. Press, Cambridge, Massachusetts U.S.A. 1966
- [22] MATLAB 2020 The MathWork Inc. Natic, MA, USA